A systematic interpretation of differential capacitance data

Nir Gavish*

Department of Mathematics, Technion - IIT, Israel

Keith Promislow†

Department of Mathematics, Michigan State University, East Lansing, MI

Abstract

Differential capacitance (DC) data has been widely used to characterize the structure of electrolyte solutions near charged interfaces and as experimental validation of models for electrolyte structure. Fixing a large class of models of electrolyte free energy that incorporate finite volume effects, a reduction is identified which permits the identification of all free energies within that class that return identical DC data. The result is an interpretation of DC data through the equivalence classes of non-ideality terms, and associated boundary layer structures, that cannot be differentiated by DC data. Specifically, for binary salts, DC data, even if measured over a range of ionic concentrations, is unable to distinguish between models which exhibit charge asymmetry, charge reversal, and even ion crowding. The reduction applies to capacitors which are much wider than the associated Debye length and to finite-volume terms that are algebraic in charge density. However, within these restrictions the free energy is shown to be uniquely identified if the DC data is supplemented with measurements of the excess chemical potential of the system in the bulk state.

* ngavish@tx.technion.ac.il

† kpromisl@math.msu.edu

I. INTRODUCTION

The contact between charged objects, such as a metal surface, macromolecule, or membrane, and an electrolyte solution results in the rearrangement of ionic distributions near the interface and formation of the so-called electric double layer. The double layer has been extensively studied due to its importance within a wide range of areas including electrochemistry, biochemistry, physiology and colloidal science. In particular, important systems such as supercapacitors, energy conversion devices or ion channels [1–5], underline the need to understand double layer structure in concentrated solutions where non-ideality of the solution due to ion-ion interactions and finite-size effects is significant.

One of the key quantities in the study of the double-layer structure is differential capacitance data, as it is readily available experimentally. A 1:1 electrolyte solution bounded by a charged wall, as shown in Figure 1, rearranges to create a region of charge imbalance within the electrolyte near the adjacent wall. The total extracted charge satisfies [6]

$$Q(\phi_0, \overline{c}) := q \int_0^\infty (p - n)\, dx,$$

where q is the unit of electrostatic charge, x is the distance from the wall, $p(x)$ and $n(x)$ are the density profiles of the cations and of the anions, respectively. The potential on the charged wall is denoted by ϕ_0, where the reference potential is taken to be zero at the bulk, i.e., $\phi(\infty) = 0$. The differential capacitance (DC) is defined as the change in $Q(\phi_0, \overline{c})$ with respect to changes in the applied potential ϕ_0,

$$C_D(\phi_0, \overline{c}) := \frac{\partial Q}{\partial \phi_0}(\phi_0, \overline{c}).$$

The local charge imbalance occurs only in the electric double layer region. Therefore, differential capacitance data provides an important indirect measurement of double layer structure. Lyklema [7], for example, states *"Quotients of charges and potentials, i.e. capacitances, are in principle the most eligible parameters for quantitative analysis of overcharging"*.

Previous studies have only used differential capacitance data as a validation tool, comparing DC data computed from models of electrolyte structure to experiments. The goal of this work is to quantify the ability of differential capacitance measurements to differentiate between models of electrolyte free energy by characterizing *all* models, within a family, which recover prescribed differential capacitance data.

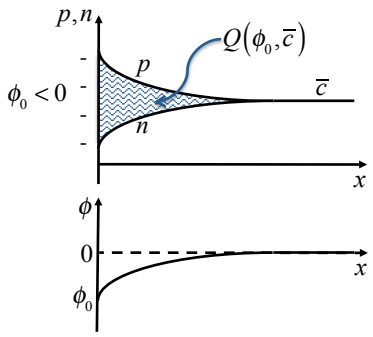

FIG. 1. Illustration of the system of study. An electrolyte solution is bounded by a hard wall. Here, for example, the wall is negatively charged. Top graph presents the density profiles of the cations and of the anions, denoted by $p(x)$ and $n(x)$, respectively. The concentration of both ionic species at the bulk equals $\bar{c}$. The area captured between the profiles is proportional to the total local charge imbalance in the electrolyte $Q(\phi_0, \bar{c})$, which balances the surface charge on the wall. The bottom graph presents the potential $\phi(x)$.

This issue is addressed within a general variational framework of Poisson-Boltzmann type free energy models

$$\mathcal{E} = \int k_B T \left[\underbrace{p\left(\ln\frac{p}{c^o} - 1\right) + n\left(\ln\frac{n}{c^o} - 1\right)}_{\text{entropy}} + \underbrace{f(p,n)}_{\text{non-ideality}} \right] + \underbrace{q(p-n)\phi - \frac{1}{2}\epsilon|\nabla\phi|^2}_{\text{electrostatic}}\, dx, \quad (1)$$

where k_B is the Boltzmann constant, T is the temperature and the algebraic term $f(p,n)$ represents the entropy correction due to non-ideality caused by ion-ion interactions at concentrated solutions [8]. In the case of an ideal solution, i.e., $f(p,n) \equiv 0$, the action reduces to the classic Poisson-Boltzmann model. The corresponding generalized Poisson-Boltzmann equations arise as the critical point equation for the action (Hamiltonian) subject to a total mass constraint on each charged species, see Section 2 of [9]. Indeed, setting the variations of the Hamiltonian with respect to ϕ, p and n to zero, while properly handling the infinite interval [10], yields the system,

$$\begin{aligned} &\epsilon\phi''(x) + q(p-n) = 0, && \text{(Poisson)} \\ &\ln\tfrac{p}{\bar{c}} + f_p(p,n) + \tfrac{q}{k_B T}\phi = f_p(\bar{c},\bar{c}), \\ &\ln\tfrac{n}{\bar{c}} + f_n(p,n) - \tfrac{q}{k_B T}\phi = f_n(\bar{c},\bar{c}), && \text{(generalized Boltzmann)}, \end{aligned} \quad (2a)$$

$$\phi(0) = \phi_0, \quad \phi(\infty) = 0, \quad p(\infty) = n(\infty) = \bar{c}, \quad (2b)$$

where the partial deriviatives $f_p(\bar{c},\bar{c}) := \frac{\partial}{\partial p} f(p,n)\Big|_{p=n=\bar{c}}$ and $f_n(\bar{c},\bar{c}) := \frac{\partial}{\partial n} f(p,n)\big|_{p=n=\bar{c}}$ are Lagrange multipliers which are associated with mass conservation.

The goal of this paper is to identify, within this framework, all non-ideality functions f which recover a prescribed differential capacitance data. In particular to show that DC data cannot distinguish between models with and without charge reversal effects or between models with and without anion-cation asymmetries. More specifically, a unique determination of the free energy requires the prescription of two functions $A(\bar{c})$ and $B(\bar{c})$ which characterize the concentration-dependent single-ion activity coefficients, that is the dependence of the excess chemical potentials $\mu_\pm$ on the ionic density under bulk conditions $p \equiv n \equiv \bar{c}$. Complementary measurements of double-layer structure, such as optical measurements utilizing second harmonic generation phenomena [11, 12], can be employed to probe the domain of validity of the constant-dielectric Hamiltonian framework (1).

The method permits a recovery of the theoretical models presented in Figure 2 from their differential capacitance data and at the same time a derivation of alternative models which give rise to identical differential capacitance data. As an application, the experimental data of Valette [13] for a KPF_6 electrolyte solution in contact with a silver single crystal electrodes is recovered from *two models with distinct boundary layer structures*.

Previous studies [9, 14–24] have presented free energies which correspond to specific choices of the non-ideality function f within the framework (1). These models can provide qualitative agreement between numerically derived differential capacitance data and experimental data, see Figure 2. Similar qualitative agreement is achieved by models within different frameworks that account, for example, for the dependence of the dielectric constant upon the electric field [25, 26] and/or the dependence of the dielectric constant upon the local ionic concentration [24, 27–29], see [30] (for a review). It is possible to adapt the method presented here to characterize the models within these frameworks which provide prescribed differential capacitance data.

II. REFORMULATION OF THE MODEL

It is instructive to consider a system of a 1:1 electrolyte bounded between two walls located at $x = 0$ and $x = L$ such that the electric potential on the walls is $\phi(0) = \phi_0$ and $\phi(L) = -\phi_0$. In this case, the generalized Poisson-Boltzmann system is of the form (2a)

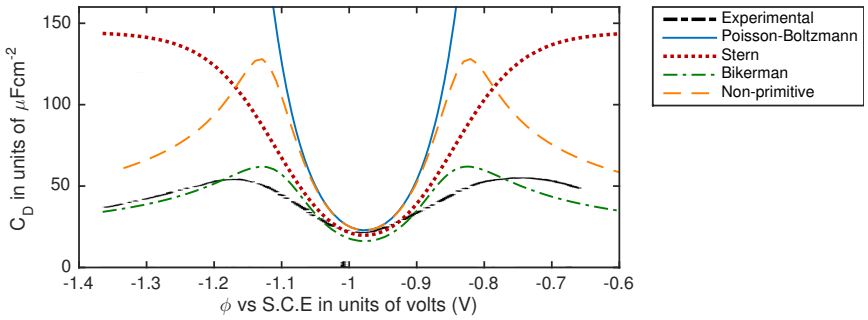

FIG. 2. Experimentally measured differential capacitance curve for a solution of $0.01M$ KPF_6 adapted from Figure 3 of [13] (Black dashed-dotted curve) and corresponding theoretical predictions by the Poisson-Boltzmann model (2) with $f \equiv 0$ (solid blue), Gouy-Chapmann-Stern with a Stern layer of width $d = 0.157nm$ (red dots), Bikerman model with $\nu = 0.02$ (a parameter associated with the closest packing density of the ions), and the non-primitive model with (32) and excess polarization parameters $\alpha_n = \alpha_p = 0.1$ (Dashed orange). Note models which better agree with experimental data do exist in the literature.

with the boundary conditions

$$\phi(0) = \phi_0, \quad \phi(L) = -\phi_0, \quad \frac{1}{L}\int_0^L p(x)\,dx = \frac{1}{L}\int_0^L n(x)\,dx = \bar{c}. \tag{3}$$

At the large width limit $L \to \infty$, this system reduces to the generalized Poisson-Boltzmann system (2) [10].

The generalized Boltzmann equations in (2) can be written in the form

$$\mu_\pm^{\text{ideal}} + \mu_\pm^{\text{excess}} = \mu_\pm^{\text{excess}}(\bar{c}, \bar{c}), \tag{4a}$$

where the standard ideal electrochemical potential is defined as

$$\mu_+^{\text{ideal}} := \ln\frac{p}{\bar{c}} + \frac{q}{k_B T}\phi, \quad \mu_-^{\text{ideal}} := \ln\frac{n}{\bar{c}} - \frac{q}{k_B T}\phi, \tag{4b}$$

and the excess electrochemical potential is defined as

$$\mu_+^{\text{excess}} := f_p(p, n), \quad \mu_-^{\text{excess}} := f_n(p, n). \tag{4c}$$

For simplicity, the system (4), together with Poisson's equation in (2), is non-dimensionalized by scaling

$$\tilde{\phi} = \frac{q}{k_B T}\phi, \quad \tilde{x} = \frac{x}{\lambda_D}, \quad \tilde{p} = \frac{p}{c^o}, \quad \tilde{n} = \frac{n}{c^o}, \quad \tilde{\bar{c}} = \frac{\bar{c}}{c^o}, \quad \tilde{L} = \frac{L}{\lambda D}, \quad \lambda_D = \sqrt{\frac{k_B T \epsilon}{q^2 c^o}}, \tag{5}$$

where λ_D is the Debye length. Further, making the change of variables from ionic densities n and p to net charge density $\rho = n - p$ and total mass density $c = n + p$, and denoting the overall entropy by

$$h(p, n) := [p(\ln p - 1) + n(\ln n - 1)] + f(p, n), \tag{6}$$

yields the non-dimensional system (written after dropping the tildes)

$$\phi''(x) = \rho, \tag{7a}$$

$$\begin{aligned} h_c(c, \rho) &= h_c(2\overline{c}, 0), \\ h_\rho(c, \rho) &= \phi + h_\rho(2\overline{c}, 0), \end{aligned} \tag{7b}$$

subject to boundary conditions

$$\phi(0) = \phi_0, \quad \phi(L) = -\phi_0. \tag{7c}$$

Note that typically the reference density c^o in (5) is set as the bulk density $\bar{c}$. Such a choice would eliminate the explicit appearance of $\bar{c}$ in (7). We choose, instead, an arbitrary reference density as a central role is played by the relationship which connects the bulk density $\bar{c}$ to the Lagrange multipliers.

The system (7) defines the generalized Poisson-Boltzmann framework. We add to the framework (7) an additional constraint that $h(c, \rho)$ is strictly convex. As will be discussed in the next section, this constraint is required to assure well-posedness of (7). From a physical perspective, it assures that the system reaches a single uniform state in the absence of applied voltage or in the bulk, as expected for systems with a single solvent such as those considered in this work. We note that this assumption is unlikely to globally hold for more complex systems with mixture of solvents and antagonistic salts.

III. THE LARGE WIDTH LIMIT: INCORPORATION OF THE DIFFERENTIAL CAPACITANCE DATA

Traditionally, the differential capacitance data predicted by a generalized PB model is computed by solving the PB equations for the charge density profiles for each desired applied voltage, integrating the spatial dependence of the charge densities, and then differentiating the result with respect to applied voltage. The procedure is computationally inefficient

and hides the underlying structure relating the generalized PB equation to the differential capacitance data. Thus, a prerequisite for systematically interpreting differential capacitance data is to analytically resolve the forward problem, yielding an explicit connection between the differential capacitance data and a given generalized Poisson-Boltzmann model.

In a companion paper [10], we address the resolution of the forward problem in a more general framework. For completeness, in this section we derive the results for the case (7). The generalized Poisson-Boltzmann model (7) is well-defined only when equations (7b) implicitly define $c(\phi, \bar{c})$ and $\rho(\phi, \bar{c})$. These requirements are met when $h(c, \rho)$ is strictly convex [10, Lemma 1]. This result implies that for each well-defined generalized Poisson-Boltzmann model (7), Poisson's equation (7a) can be written as an autonomous equation $\phi''(x) = \rho(\phi, \bar{c})$. Setting $E := \phi'(x)$ yields the dynamical system

$$\begin{aligned} \phi'(x) &= E, \\ E'(x) &= \rho(\phi; \bar{c}). \end{aligned} \tag{8}$$

The system has a fixed-point at $(0, 0)$ which is a saddle point (see Lemma 2 in [10]), that corresponds to the bulk state of the electrolyte system. The double layer boundary structure corresponds to the stable-manifold trajectory Γ that starts from a point (ϕ_0, E_0) on the line $\phi = \phi_0$ and reaches the line $\phi = -\phi_0$ at $x = L$, see Figure 3A. In the wide-capacitor limit, $L \to \infty$, this latter condition requires that Γ approaches the saddle point $(0, 0)$ as $x \to \infty$, see Figure 3B. This reduction is very significant, as it renders Γ independent of the value of ϕ_0: it becomes a "bulk relation" that is valid in the interior domain, indeed Γ can be parameterized by the relation, $(\phi, E(\phi))$, where the 'Dirichlet-to-Neumann' map $E = E(\phi)$ satisfies

$$\frac{dE}{d\phi}(\phi) = \frac{\rho(\phi; \bar{c})}{E(\phi)}, \qquad E(0) = 0. \tag{9}$$

The independence of the Dirichlet-to-Neumann map, $E(\phi, \bar{c})$ to ϕ_0, allows the boundary data ϕ_0 to be replaced with the electric potential ϕ, which yields an explicit relation between the total charge for the differential capacitance. Indeed, substituting the LHS of Poisson's equation (7a) in the expression for the overall local charge imbalance in the electrolyte yields

$$Q(\phi_0) = \int_0^\infty \rho(x; \phi_0, \bar{c})\, dx = -\int_0^\infty \phi_{xx}(x; \phi_0, \bar{c})\, dx = \phi_x(x; \phi_0, \bar{c})|_{x=0} = E(\phi, \bar{c})|_{\phi=\phi_0}. \tag{10}$$

Replacing ϕ for ϕ_0, and using (9), yields the expression

$$C_D(\phi) = \frac{dE}{d\phi}(\phi) = \frac{\rho(\phi, \bar{c})}{E(\phi)}, \tag{11}$$

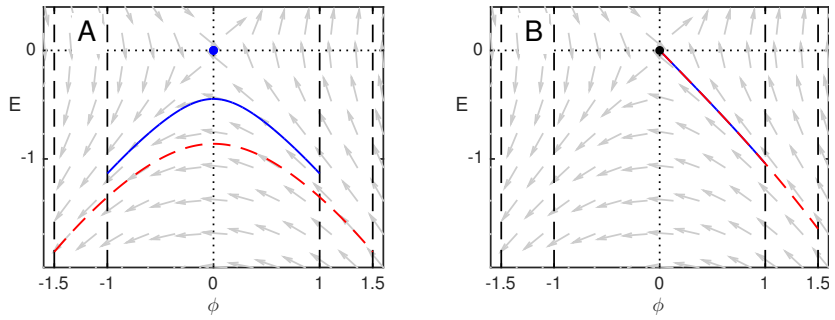

FIG. 3. Trajectories of the Poisson-Boltzmann dynamical system (8) corresponding to $\phi_0 = 1$ (solid) and $\phi_0 = 1.5$ (dash-dotted) in the cases A: Electrolyte bounded between two walls located at $x = 0$ and $x = L = 2$ such that the electric potential on the walls is $\phi(0) = \phi_0$ and $\phi(L) = -\phi_0$. and B: The limiting case, $L = \infty$, for which an electrolyte is bounded by a charged wall such that the electric potential on the wall is $\phi(0) = \phi_0$, and the potential at the bulk is $\phi(\infty) = 0$.

or, via (10), equivalently

$$\rho(\phi; \overline{c}) = Q(\phi; \overline{c}) C_D(\phi; \overline{c}). \tag{12}$$

Moreover, the function $\rho(\phi; \overline{c})$ is invertible with respect to ϕ, defining $\phi = \phi(\rho, \overline{c})$.

Lemma 1. *The function ρ defined in (12) satisfies $\rho_\phi > 0$, and is invertible with respect to ϕ for fixed values of $\overline{c}$.*

Proof. See proof of Lemma 2 in [10]. Note that the proof relies on the strict convexity of $h(c, \rho)$. □

Relation (12) and Lemma 1 imply that the differential capacitance, an externally measured quantity, slaves the local potential ϕ to the local charge imbalance, ρ, and the bulk salt concentration. This interpretation *opens the way to the systematic analysis of the differential capacitance data.*

IV. DC DATA AS ACTION CONSTRAINT

A fundamental step in understanding DC data is to identify the constraints it imposes on the local free energy density functions $h(c, \rho)$, for which the corresponding generalized Poisson-Boltzmann model (7) yields the prescribed data. The key element of this process is

to realize that relation (12) can be extended to an invertible relation that slaves ϕ and $\bar{c}$ to the binary densities.

Lemma 2. *The generalized Boltzmann equations* (7b) *uniquely define inverse relations*

$$\begin{aligned} \phi &= \phi(c, \rho), \\ \bar{c} &= \bar{c}(c, \rho). \end{aligned} \tag{13}$$

In particular,for a capacitor in the semi-infinite regime, with a prescribed free energy of the (1)*, knowing the exposed charge* $\rho(x)$ *and total charge* $c(x)$*, a point* x *determines the voltage* $\phi(x)$ *and the bulk charge density* $\overline{c}$*.*

Proof. The proof relies on the strict convexity of $h(c, \rho)$, see Appendix A. □

For clarity of presentation the right-hand side of the Boltzmann equations (7b) may be rewritten in the form

$$\begin{aligned} h_c(\rho, c) &= A\left(\overline{c}(c, \rho)\right), \\ h_\rho(\rho, c) &= \phi(\rho, \overline{c}(c, \rho)) + B\left(\overline{c}(c, \rho)\right), \end{aligned} \tag{14}$$

where the bulk data, A and B, which arise as Lagrange multipliers, represent the chemical potentials,

$$A(\overline{c}) := h_c(2\overline{c}, 0), \quad B(\overline{c}) := h_\rho(2\overline{c}, 0), \tag{15}$$

of the system in the bulk state $\rho = 2\overline{c}$ and $Q = 0$. The bulk data can also be related to the excess chemical potentials

$$A(\overline{c}) = \frac{1}{2}\left[\mu_+^{\text{excess}}(\overline{c}) + \mu_-^{\text{excess}}(\overline{c})\right], \quad B(\overline{c}) = \frac{1}{2}\left[\mu_+^{\text{excess}}(\overline{c}) - \mu_-^{\text{excess}}(\overline{c})\right].$$

The construction energy densities h which recover the prescribed differential capacitance data, reduces to finding convex h that satisfy (14). The smoothness of h requires the agreement of its mixed partials $h_{\rho Q} = h_{Q\rho}$. In view of the slaving relation (13), equating the ρ and Q partial derivatives of (14) yields the compatibility condition

$$h_{c\rho} = A'(\overline{c})\overline{c}_\rho = \phi_{\overline{c}}\overline{c}_c + B'(\overline{c})\overline{c}_c = h_{\rho c}, \tag{16}$$

which is equivalent to the first-order system for $\bar{c}$,

$$\begin{pmatrix} -\phi_{\overline{c}} - B'(\overline{c}) \\ A'(\overline{c}) \end{pmatrix} \cdot \begin{pmatrix} \overline{c}_c \\ \overline{c}_\rho \end{pmatrix} = 0. \tag{17}$$

For prescribed *bulk* data $A(\bar{c})$ and $B(\bar{c})$, the compatibility condition (17) provides an explicit evaluation for the $\bar{c} = \bar{c}(c, \rho)$ relation subject to the boundary data $\bar{c}(c, 0) = c/2$ which follows from the bulk assumption $\rho = 0$ and $c = 2\bar{c}$. Bulk data that yield a smooth h in an open domain D containing the bulk data line $\{\rho = 0,\, c > 0\}$ are called *admissible*. We unfold the requirements of admissibility in the sequel.

The system (17) is readily solvable by the method of characteristics: $\bar{c}$ is constant along lines $(\rho, c) = (c(t, s), \rho(t, s))$ where

$$\frac{\partial}{\partial t}\begin{pmatrix} c(t,s) \\ \rho(t,s) \end{pmatrix} = \begin{pmatrix} -\phi_{\bar{c}}(\rho, s) - B'(s) \\ A'(s) \end{pmatrix}, \quad \begin{pmatrix} c(0,s) \\ \rho(0,s) \end{pmatrix} = \begin{pmatrix} 2s \\ 0 \end{pmatrix}. \tag{18}$$

A first requirement of admissibility is that the free data, prescribed on the line $(c, \rho) = (2s, 0)$, be non-characteristic. For the system (18) this is equivalent to the condition

$$A'(s) \neq 0, \quad s > 0. \tag{19}$$

Subject to the condition (19), we obtain the characteristic curves,

$$\begin{aligned} \rho(s,t) &= A'(s)t, \\ c(s,t) &= 2s - \frac{\Phi_{\bar{c}}\left(A'(s)t, s\right)}{A'(s)} - B'(s)t, \end{aligned} \tag{20}$$

where we have introduced,

$$\Phi_{\bar{c}}(\rho, \bar{c}) = \frac{d}{d\bar{c}} \int_0^\rho \phi(s, \bar{c}) ds.$$

The function $\phi = \phi(s, \bar{c})$ is obtained by inverting (12). Eliminating s and t from (20) yields the relation

$$c(\rho, \bar{c}) = 2\bar{c} - \frac{\Phi_{\bar{c}}\left(\rho, \bar{c}\right) + \rho B'(\bar{c})}{A'(\bar{c})}. \tag{21}$$

To invert (21) to obtain $\bar{c} = \bar{c}(\rho, c)$ we impose a second admissibility condition,

$$\rho_{\bar{c}} := \frac{\partial}{\partial \bar{c}} \left(2\bar{c} - \frac{\Phi_{\bar{c}}\left(\rho, \bar{c}\right) + \rho B'(\bar{c})}{A'(\bar{c})} \right) > 0, \tag{22}$$

for all $\bar{c} > 0$ and for all ρ. Note that the admissibility conditions (19,22) imply strict convexity of h, see Appendix B. These admissibility conditions, however, do not uniquely determine the bulk data A and B. The result is a wide class of families of admissible models which yield the prescribed differential capacitance data, differing only in their excess chemical potential at the bulk.

The steps to construct h given the differential capacitance C_D and the bulk data A and B, are summarized below:

Inverse procedure: For a prescribed differential capacitance data $C_D(\phi, \bar{c})$,

1. Compute
$$\rho(\phi, \bar{c}) = C_D(\phi, \bar{c}) \int_0^{\phi} C_D(s, \bar{c}) ds.$$

2. Invert $\rho = \rho(\phi, \bar{c})$ from (12) with respect to ϕ to obtain $\phi = \phi(\rho, \bar{c})$.

3. Compute
$$\Phi_{\bar{c}} = \frac{d}{d\bar{c}} \int_0^{\rho} \phi(s, \bar{c}) ds.$$

4. For any admissible pair $A(\bar{c})$ and $B(\bar{c})$ define
$$\rho(\rho, \bar{c}) := 2\bar{c} - \frac{\Phi_{\bar{c}}(\rho, \bar{c}) + \rho B'(\bar{c})}{A'(\bar{c})}.$$
In particular this requires that $A' \neq 0$.

5. Invert $c(\rho, \bar{c})$ with respect to $\bar{c}$ to obtain $\bar{c} = \bar{c}(c, \rho)$.

6. Substite $\bar{c}(c, \rho)$ into (14) and compute the free energy $\mathcal{E}$ by integration of h_c and h_ρ to yield $h(c, \rho)$.

V. THE POISSON-BOLTZMANN DIFFERENTIAL CAPACITANCE DATA

It is well known that the Poisson-Boltzmann (Gouy-Chapmann) model, that is (7) with $f \equiv 0$, gives rise to the differential capacitance

$$C_D^{PB}(\phi, \bar{c}) = \sqrt{\bar{c}} \cosh \frac{\phi}{2}. \tag{23}$$

In this section we apply the inverse process to recover the Poisson-Boltzmann model and families of alternative models which yield the same differential capacitance data C_D^{PB}. Applying the inverse procedure with $C_D^{PB}(\phi, \bar{c})$, yields the density, see step 4,

$$c(\rho, \bar{c}) = 2\bar{c} - \frac{2\left[1 - \sqrt{1 + (\rho/2\bar{c})^2}\right] + \rho B'(\bar{c})}{A'(\bar{c})}. \tag{24}$$

For simplicity, we consider bulk data in the form

$$A'(\bar{c}) = \frac{\alpha}{\bar{c}}, \quad B'(\bar{c}) = 0, \tag{25}$$

for which the density reduces to

$$c = \left[\frac{2(\alpha - 1) + 2\sqrt{1 + (\rho/2\bar{c})^2}}{\alpha} \right] \bar{c}. \tag{26}$$

This relation is uniquely invertible for $\bar{c} > 0$ for all $\alpha \geq 1$,[31]

$$\bar{c} = \frac{(\alpha^2 - \alpha)c - \sqrt{\alpha^2\rho^2 + (\alpha^2 - 2\alpha)\rho^2}}{2(\alpha^2 - 2\alpha)}. \tag{27}$$

A. Recovery of the Poisson-Boltzmann model

The choice $\alpha = 1$ in (25) leads to the traditional Poisson-Boltzmann model. Indeed, in this case, see (27),

$$\bar{c} = \frac{1}{2}\sqrt{c^2 - \rho^2}. \tag{28}$$

Substituting this expression for $\bar{c}(c, \rho)$, as well as the choices (25), in (14) yields

$$h_c(c, \rho) = \log \frac{\sqrt{c^2 - \rho^2}}{2}, \qquad h_\rho(c, \rho) = \log \sqrt{\frac{c + \rho}{c - \rho}}. \tag{29}$$

Making the change of variables from (c, ρ) to ionic densities (p, n) gives $h_p(p, n) = \log p$ and $h_n(p, n) = \log n$. Integration of the system, subject to the normalization $h(\bar{c}, \bar{c}) = 0$, yields the entropic component of the free energy of the Poisson-Boltzmann model, see (1), and recovers the Poisson-Boltzmann model from its differential capacitance data.

B. Derivation of an alternative model

Choices of $\alpha \neq 1$ in (25) yields alternative free energies which recover the same differential capacitance data (23) as the Poisson-Boltzmann model. For $\alpha = 3/2$, (27) reduces to

$$\bar{c} = \sqrt{c^2 - \rho^2/3} - \frac{\rho}{2}, \tag{30}$$

and the corresponding free energy function $h_{\alpha=3/2}$ can be computed from (14), see Figure 4A. In Figure 4B displayed the charge densities for the case $\phi_0 = 1$. We observe the charge densities are both positive, and they differ from the charge densities predicted by the Poisson-Boltzmann model. We stress again the point that the *differential capacitance data is the same for both choices of* $\alpha = 1$ *and* $\alpha = 3/2$ in Figure 4B.

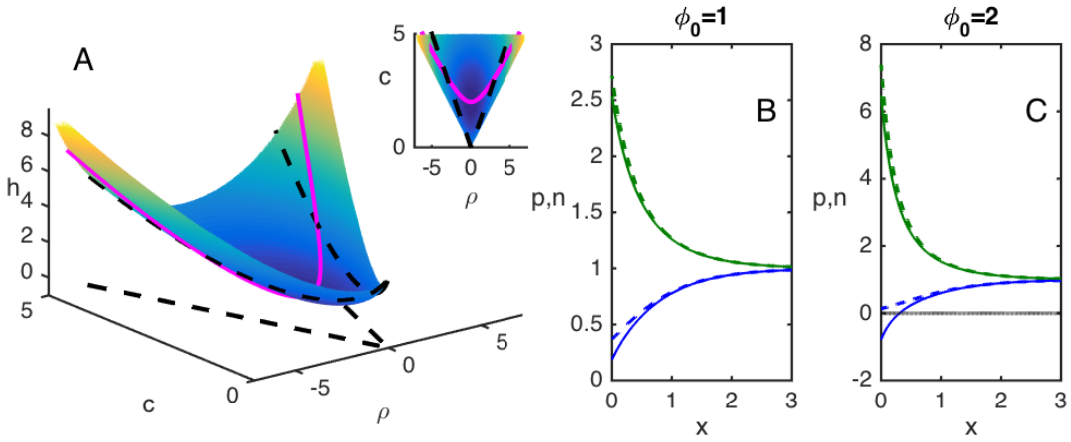

FIG. 4. (color online) A: The surface $h_{\alpha=3/2}(c,\rho) - h_{\alpha=3/2}(2\overline{c},0)$ computed for $\overline{c}=1$, and the trajectory $(\rho, c(\rho,\overline{c}=1))$ (solid magenta curve). The subplot presents the same data viewed from above. Black dashed lines are $c=|\rho|$. B and C: The charge density profiles $p(x)$ (bottom solid curve) and $n(x)$ (top solid curve) corresponding to the case $\alpha=3/2$ and for an applied voltage $\phi_0=1$ in B and $\phi_0=2$ in C. Also plotted are the charge density profiles of the Poisson-Boltzmann model $\alpha=1$ (dotted curves).The positive charge density profile in C is negative near the wall and therefore non-physical.

C. Domain of the free energy density function h

For the Poisson-Boltzmann energy,with $\alpha=1$, the domain where h is smooth coincides with the physical domain $\rho \geq |c|$, for which $p,n \geq 0$.

Significantly, the characteristic domain of h is determined by the choice of the free data A and B, and does not necessarily coincide with the natural domain. Indeed, the function $h(c,\rho)$ looses smoothness when two characteristics emanating from the line $\{(2\overline{c},0)\big|\,\overline{c}>0\}$ intersect at a point (c,ρ) off of the line, see relation (14) and also Figure 5A. For example, the curve $c(\rho;\overline{c}=1)$ in Figure 5B corresponds to the characteristic emanating from $(2,0)$. Specifically, one expects that $c_{\overline{c}}>0$ and thus the boundary of the characteristic domain of h consists of the characteristic (c^0,ρ^0) emanating from $(2\overline{c},0)$ where $\overline{c}\to 0$. By (26), this characteristic satisfies

$$c^0 := \lim_{\overline{c}\to 0} c(\overline{c},\rho) = \frac{|\rho|}{\alpha}. \tag{31}$$

At the boundary, h is no longer smooth, see (29) and also Figure 5C.

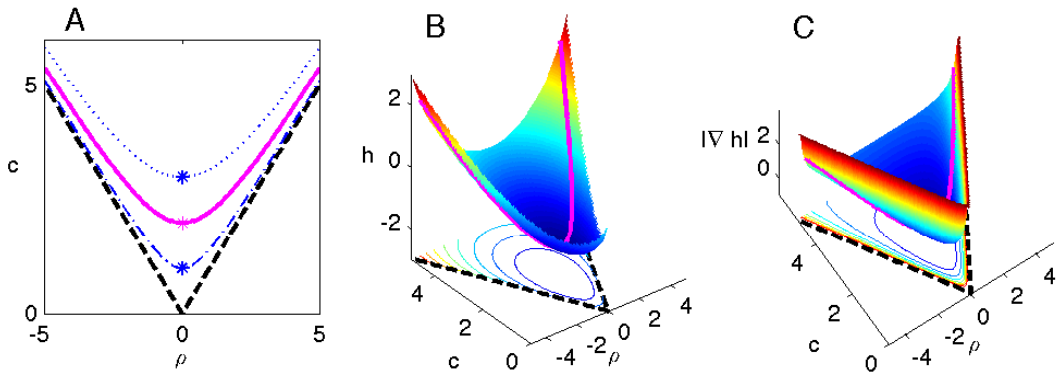

FIG. 5. (color online) A: Characteristics (c, ρ) defined by (26) where $\alpha = 1$, emanating from $(2\overline{c}, 0)$ where $\overline{c} = 0.5$ (dash-dots), $\overline{c} = 1$ (solid magenta curve) and $\overline{c} = 1.5$ (dotted). B: The normalized function $h_{PB} - h_{PB}(2\overline{c}, 0)$ where $\overline{c} = 1$. C: The gradient $|\nabla h_{PB}|$, see (29). Solid magenta curve in A and B is the trajectory $(\rho, c(\rho, \overline{c} = 1))$, corresponding to the characteristic curve emanating from $(2, 0)$. Black dashed lines in all graphs are $c = \pm\rho$.

The choice $\alpha = 3/2$ leads to the action $h_{\alpha=3/2}(c, \rho)$ which is smooth in the admissible domain $c > \frac{2}{3}|\rho|$, see Figure 4A. This admissible domain is larger than the region of physically admissible solutions. Accordingly, solutions of the corresponding generalized Poisson-Boltzmann system with $\alpha = 3/2$ are not confined to the physical region of positive charge densities, see, e.g., Figure 4A. In Figure 4C we plot the spatial profiles $n(x)$ and $p(x)$ for $\phi_0 = 2$, and observe that $p(x) < 0$.

D. An alternative model with charge reversal

To construct models which are valid for low enough ionic concentration, we require that the free data agrees with the PB free data at low ionic concentrations, when $\overline{c} = 0$. Specifically we consider $A'(\overline{c}) = a(\overline{c})/\overline{c}$ and $B'(\overline{c}) = b(\overline{c})$ where a and b are smooth functions satisfying $a(0) = 1$ and $b(0) = 0$. Such choices of free data interpolates between the PB data, i.e. $\alpha = 1$ in (25), at low bulk concentrations while incorporating non-ideal behavior at high bulk concentrations. As a specific example we choose,

$$A'(\overline{c}) = \frac{1 + \alpha\overline{c}}{1 + \overline{c}} \frac{1}{\overline{c}}, \quad B'(\overline{c}) = 0.$$

Within this framework the value $\alpha = 1/2$ yields the density, see (24),

$$c = 2\frac{(1+\overline{c})\sqrt{\rho^2 + 4\overline{c}^2} - \overline{c}^2}{2+\overline{c}}.$$

For this value of α, we may verify that $c_{\overline{c}} \neq 0$ for all $|\rho| < \rho_*$ where $\rho^* > 16$. Therefore, this model breaks-up only at very high voltages or concentrations which lead to excessive local charge imbalance $|\rho| > \rho^* \gg 1$ and to a non-smooth free energy. Within the validity range $|\rho| < \rho^*$, the model give rises to strictly positive charge densities.

Figure 6A presents the free energy density function h, as well as the curve $\rho(Q; \overline{c} = 1)$. The action is defined for $c > |\rho|$. Figure 6B presents the curve for $\overline{c} = 1$ in (p, n) coordinates. In contrast to the previous cases, the curve $(n, p(n; \overline{c} = 1))$ is not a function of n. Accordingly, the charge profiles are non-monotone for large applied voltage, see Figures 6C and 6D.

The non-monotone charge profile in Figure 6D provides an example of *charge reversal* or *over-charging*, a phenomenon in which the electric double layer region contains more countercharge than is needed to compensate the surface charge. This phenomena has been recognized and studied since the 1940s, see [7] and references within for a review. The precise physical or chemical reasons for over-charging are still debated [32], but it is widely believed that over-charging is related to asymmetries between anions and cations in their interactions with the surface. Extensive study has been dedicated to derive generalized Poisson-Boltzmann models that can describe overcharging, see [33] for a review. These models commonly take into account asymmetric finite size effects, e.g., using the hyper-netted-chain/mean-spherical approximation (HNC/MSA) approach.[34]

The model corresponding to the free energy density function $h_{\alpha=1/2}$ is a simple generalized Poisson-Boltzmann model that describes overcharging. Interestingly, it is a symmetric model, i.e., $h(p, n) = h(n, p)$ [35], showing that over-charging need not necessarily originate from asymmetries between ionic species.

E. An alternative model with asymmetry

The Poisson-Boltzmann differential capacitance data, C_D^{PB} is symmetric (i.e., an even function) with respect to ϕ. Therefore, it is reasonable to expect that the model yielding C_D^{PB} would also be symmetric, i.e., negative and positive charge satisfy $h(p, n) = h(n, p)$. Indeed, the three models presented previously in this section are all symmetric in this sense. How-

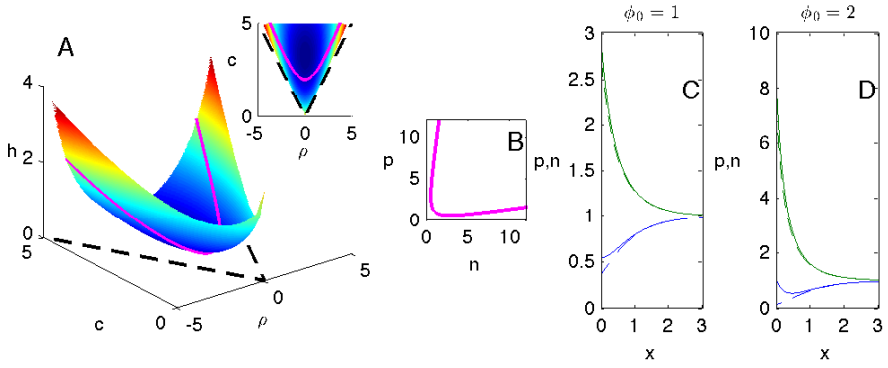

FIG. 6. (color online) A: The surface $h_{\alpha=1/2}(c,\rho) - h_{\alpha=1/2}(2\bar{c},0)$ computed where $\bar{c}=1$, and the trajectory $(\rho, c(\rho,\bar{c}=1))$ (solid). The subplot presents the same data viewed from above. Black dashed lines are $c|\rho|$. B: The trajectory $(\rho, c(\rho,\bar{c}=1))$ from A (solid), but in (p,n) coordinates. C and D: The charge density profiles $p(x)$ (bottom solid curve) and $n(x)$ (top solid curve) corresponding to the case $\alpha = 1/2$ and for $\phi_0 = 1$ in C and $\phi_0 = 2$ in D. Also plotted are the charge density profiles of the Poisson-Boltzmann model $\alpha = 1$ (dotted curves).

ever, somewhat surprisingly, we may derive asymmetric models which recover the symmetric differential capacitance data C_D^{PB}. Indeed, the particular choice $A' = \frac{1}{\bar{c}}$ and $B' = \frac{1}{3\bar{c}}$, yields an asymmetric action h whose characteristic boundaries are the lines $c = 2\rho/3$ for $\rho > 0$ and the line $\rho = 4\rho/3$ for $\rho < 0$.

In Figure 7A we plot the corresponding action h, which is visibly asymmetric. In Figure 7B we plot the charge density profiles for the applied voltage $\phi_0 = -1$, and in Figure 7C we plot the charge density profiles for $\phi_0 = 1$. It can be seen that the charge profiles differ between the cases, manifesting the asymmetries between the charges. The changes are also qualitative - applying negative potential leads to charge inversion, while positive potential presents similar behavior to the model of Figure 4 [36]. Nevertheless, the area captured between the two profiles is identical and equals 1.4739.

VI. APPLICATION TO COMMON MODELS

The inverse procedure may be applied to study common extensions of the Poisson-Boltzmann model for the double layer structure, such as the Gouy-Chapman-Stern model

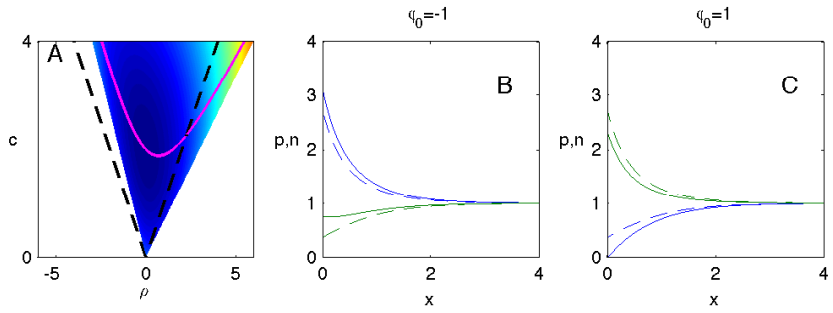

FIG. 7. (color online) A: The surface $h_{\alpha=1,\beta=1/3}(c,\rho) - h_{\alpha=1,\beta=1/3}(2\overline{c},0)$ computed where $\overline{c}=1$, and the trajectory $(\rho, c(\rho,\overline{c}=1))$ (solid magenta curve). Black dashed lines are $c=|\rho|$. B: The charge density profiles $p(x)$ (top solid curve) and $n(x)$ (bottom solid curve) for $\phi_0=-1$. C: The charge density profiles $p(x)$ (bottom solid curve) and $n(x)$ (top solid curve) for $\phi_0=1$. Also plotted are the charge density profiles of the Poisson-Boltzmann model $\alpha=1$ (dashed curves).

or the Bikerman model.

A. The Gouy-Chapman-Stern model

The Gouy-Chapman-Stern model [17] is a modification of the Poisson-Boltzmann (Gouy-Chapman) model to account for finite-size of the ions by incorporating some distance of closest approach of ions to the surface. As a consequence, the immediate layer near the electrode, the Stern layer, is free of charge. The differential capacitance C_D^{GCS} predicted by the model is given by

$$C_D^{GCS}(\phi_0,\overline{c};d) = \frac{\sqrt{2\overline{c}}\cosh(\phi/2)}{1+d\sqrt{2\overline{c}}\cosh(\phi/2)}.$$

We note that the Gouy-Chapman-Stern model is *not* a generalized Poisson-Boltzmann model of the form (7) as the Stern layer is modeled by changing the boundary condition for ϕ at $x=0$ in (7) to a Robin boundary condition. The inverse procedure can be used to obtain a generalized Poisson-Boltzmann model which recovers the Gouy-Chapman-Stern differential capacitance data C_D^{GCS}. For example, applying the inverse procedure with the choices $A=\log\overline{c}$ and $B=0$ gives rise to a generalized PB model whose corresponding action $h(c,\rho)$ is defined in the domain $c>|\rho|$ of physical validity, see Figure 8. Note that although this model yields the Gouy-Chapman-Stern differential capacitance data, the

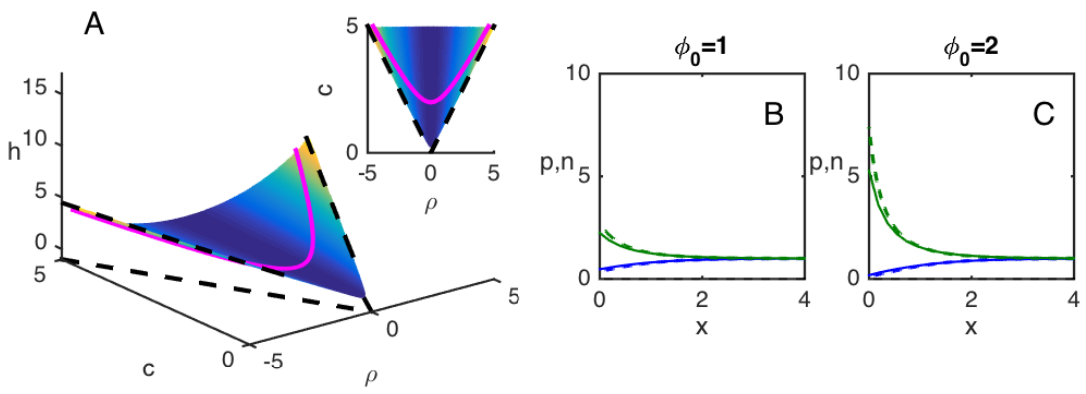

FIG. 8. (color online) A: The surface $h_{GCS}(c,\rho) - h_{GCS}(2\bar{c},0)$ computed where $\bar{c} = 3/4$, and the trajectory $(\rho, c(\rho,\bar{c}=1))$ (solid magenta curve). The subplot presents the same data viewed from above. Black dashed lines are $c = |\rho|$. B and C: The charge density profiles $p(x)$ (bottom solid curve) and $n(x)$ (top solid curve) for $\phi_0 = 1$ in B and $\phi_0 = 2$ in C. Also plotted are the charge density profiles of the Poisson-Boltzmann model (dotted curves).

associated charge density profiles do not have a Stern layer but rather they monotonically decay from the wall, see figures 8B and 8C.

B. The Bikerman model

The Bikerman model [18] reflects a choice of entropic mixing energy, see (1), of the form

$$f(p,n) = (p+n) + \frac{1-\nu(p+n)}{\nu}\log(1-\nu(p+n)),$$

where $1/\nu$ defines a reference density associated with closest packing of the ions. The differential capacitance predicted by this model is given by the Bikerman–Freise formula,

$$C_D^{BF}(\phi,\bar{c}) = \frac{2\bar{c}\cosh\phi}{\left[1+4\bar{c}\nu\sinh^2\frac{\phi}{2}\right]\sqrt{\frac{2}{\nu}\left[\log(1+2\bar{c}\nu(\cosh\phi-1))\right]}}.$$

The inverse procedure recovers the Bikerman model with the choice

$$A'(\bar{c}) = \frac{1}{\bar{c}} + \frac{1}{\bar{c}-1/2\nu}, \quad B'(\bar{c}) = 0.$$

As in the case of the Poisson-Boltzmann model, other choices of $A(\bar{c})$ and $B(\bar{c})$ yield alternatives models which also give rise to the Bikerman–Freise differential capacitance data.

C. Non-primitive generalized Poisson-Boltzmann models

Recent studies [27, 28] have extended the Poisson-Boltzmann model by accounting for ion-solvent interactions via the dependence of the dielectric constant upon ionic concentration

$$\epsilon = \epsilon_w - \alpha_p p - \alpha_n n, \tag{32}$$

where ϵ_w is the dielectric of the solvent, and the coefficients α_n and α_p are ion-specific parameters known as the excess polarization constants. This extension of the Poisson-Boltzmann model does not fall into the framework of the generalized Poisson-Boltzmann (7) which assume the solvent is a uniform dielectric medium, i.e., $\epsilon \equiv \epsilon_w$, aka a primitive generalized Poisson-Boltzmann model.

Using the inverse procedure we can derive a (primitive) generalized Poisson-Boltzmann model of the form (7) that yields the same differential capacitance as the non-primitive models with (32). For example, the case $\alpha_p = 0.1\epsilon_w$ and $\alpha_n = 0.2\epsilon_w$, together with the choices $A = 1.5 \log \bar{c}$ and $B = 0$ give rise to an action $h(c, \rho)$, see Figure 9A.

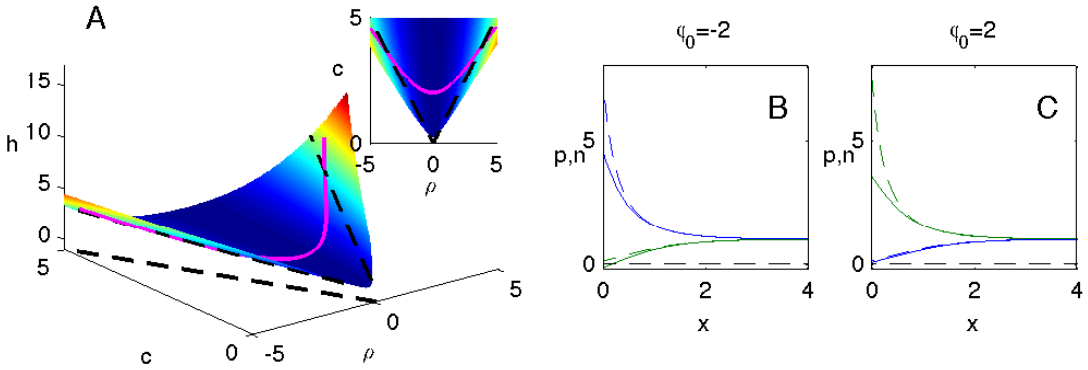

FIG. 9. (color online) A: The surface $h(c, \rho) - h(2\bar{c}, 0)$ computed where $\bar{c} = 1$, and the trajectory $(\rho, c(\rho, \bar{c} = 1))$ (solid magenta curve). The subplot presents the same data viewed from above. Black dashed lines are $c = |\rho|$. B: The charge density profiles $p(x)$ (top solid curve) and $n(x)$ (bottom solid curve) for $\phi_0 = -2$. C: The charge density profiles $p(x)$ (bottom solid curve) and $n(x)$ (top solid curve) for $\phi_0 = 2$. Also plotted are the charge density profiles of the Poisson-Boltzmann model (dotted curves).

The charge density profiles for the case $\phi_0 = -2$ and $\phi_0 = 2$ are plotted in Figures 9B

and 9C, respectively. It can be seen that the charge profiles differ between the cases, manifesting the asymmetries between the charges due to the choice $\alpha_p \neq \alpha_n$. Note that the non-primitive model (32) is mathematically valid only when the dielectric constant is positive, $\epsilon(p,n) > 0$, see (32) [37]. The validity regions of the non-primitive and primitive model do not necessarily coincide.

VII. RECOVERY OF A MODEL FROM EXPERIMENTAL DATA

The inverse procedure can be used to derive generalized Poisson-Botlzmann models that are consistent with experimentally measured differential capacitance data. Valette [13] measured differential capacitance data for a KPF_6 electrolyte solution in contact with a silver single crystal electrodes, see Figure 10A. This dataset has been a benchmark for testing the predictions of many generalized Poisson-Boltzmann models. Some of the recent models present a good agreement between this experimental data and theoretical predictions, especially in the regime of dilute solutions and small applied fields ϕ_0, see [30] for a review. Nevertheless, to the best of our knowledge, a model which accurately recovers the experimental data over its full scope is unavailable at this stage. To apply the inverse procedure,

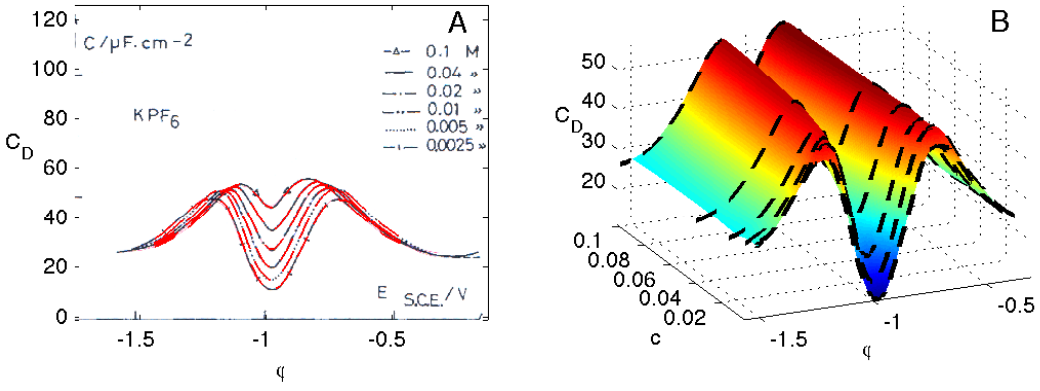

FIG. 10. A: Experimentally measured differential capacitance curves for a solution of KPF_6 at various concentrations adapted from Figure 3 of [13] (Black curves). Red curves are the model predictions for the differential capacitance data. Model predictions and experimental curves are indistinguishable). B: Same data as in A presented in $(\phi, \bar{c})$ coordinates (Black dashed curves) and surface $C_D(\phi, \bar{c})$ fitted to the data (presented in dimensional units).

we first interpolate a surface $C_D(\phi, \overline{c})$ to fit the experimental data, see Figure 10B. Then, we may *derive families of models which exactly recover the experimental differential capacitance data*. To fix the discussion we choose the bulk data in the form

$$A(\overline{c}) = \alpha \log \overline{c}, \quad B(\overline{c}) = 0.1 \log \overline{c}.$$

and present results for two choices, $\alpha = 1.5$, see Figure 11A, and $\alpha = 0.5$, see Figure 11B.

The choice $\alpha = 1.5$ gives rise to a free energy density function $h(c, \rho)$ whose domain includes the region of physically admissible solutions. Similar to the Poisson-Boltzmann case with $\alpha = 1.5$, see Figure 4, the model predicts physically admissible (positive) charge densities for small applied voltage. However, at higher applied voltages, the charge density profiles can become negative and hence non-physical.

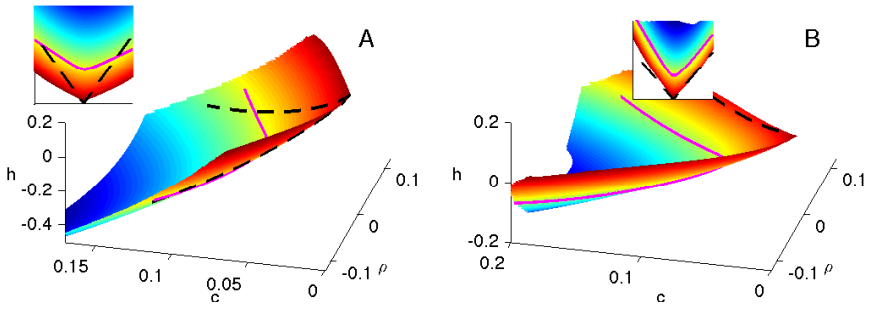

FIG. 11. (color online) The surface $h(c, \rho) - h(2\overline{c}, 0)$ computed where $\overline{c} = 0.03$, and the trajectory $(\rho, c(\rho, \overline{c} = 0.03))$ (solid magenta curve) for the choice of A: $A(\overline{c}) = 1.5 \log \overline{c}, B(\overline{c}) = 0.1 \log \overline{c}$ and B: $A(\overline{c}) = 0.5 \log \overline{c}, B(\overline{c}) = 0.1 \log \overline{c}$. The subplots in A and B presents the same data viewed from above. Black dashed lines are $c = |\rho|$.

The choice $\alpha = 0.5$ gives rise to a free energy density function $h(c, \rho)$ whose characteristic domain which roughly coincides with the physical domain, see Figure 11B. This choice gives rise to physically admissible solutions [38].

VIII. CONCLUSIONS

This study presents a procedure for systematically interpreting differential capacitance data, developing a method for recovering the entropic corrections due to non-ideality of the

solutions, and deriving generalized Poisson-Boltzmann models with prescribed differential capacitance data. The models are unique within the context of a classical uniform dielectric formulation once bulk data has been prescribed. The proposed method is demonstrated by recovering common existing models and by deriving alternative models for various sets of differential capacitance data.

The methodology presented recovers the free energy density function, i.e., the Hamiltonian of system, up to additional bulk data. The Hamiltonian provides a global description of the electrolyte behavior which is not limited to the specific, rather simple, single planar-electrode setting considered in this work. The same Hamiltonian describes electrolyte behavior in a system with more complex geometries, e.g., near a curved charged body or inside a narrow channel. In addition, it is possible to use the Hamiltonian to describe dynamics, such as arises under ionic current or time-dependent applied voltages [39].

Our study shows that differential capacitance data does not uniquely determine non-ideality or finite size effects. Indeed the methology derives families of models which all yield the same differential capacitance data, but with distinct double-layer. It is not surprising that differential capacitance data itself is insufficient to characterize double layer structure: full characterization requires several measurements. Within the Poisson-Bolzmann type framework considered here, the required complementary data can be obtained from bulk properties of the electrolyte system. However, the two data parameters $A(\overline{c})$ and $B(\overline{c})$ corresponding to the bulk excess free energy and to single ion activities are, to the best of our knowledge, unmeasurable quantities. Ultimately, an inverse method for the combined analysis of experimentally available measurements is desired.

The restriction to generalized Poisson-Boltzmann models with a uniform dielectric constant was made for simplicity of presentation. In the literature the dielectric response of a solvent is often modelled as a function of both the ionic concentration and local electric field intensity. The extension of the inverse process to incorporate this variability is straightforward, however the combination of differential capacitance data and the bulk action coefficients will not be sufficient to determine the dielectric response of the system. Therefore, additional measurements, such as impedance data or differential capacitance data in a finite gap capacitor, will likely be necessary to distinguish between models with a non-primitive dielectric response. Similarly, while it is possible to extend the inverse process to encompass non-ideality effects that are intrinsically non-local or that depend on the concentration

gradients, additional measurements will be required to distinguish between possible models. As such, this work is a first step towards a systematic interpretation of the experimental data required to determine the free energy of an electrolyte system.

Acknowledgment

The first author acknowledges support from the Technion VPR fund and from EU Marie-Curie CIG grant 2018620, while the second author acknowledges support from the NSF DMS grant 1109127 and 1409940.

Appendix A: Proof of Lemma 2

By Lemma 1 in [10], equations (7b) define the function $Q(\phi, \overline{c})$, and by the proof of Lemma 2 in [10], $\rho_\phi > 0$. Therefore, equations (7b) also define the inverse function $\phi(\rho, \overline{c})$.

Furthermore, let us rewrite equations (7b) as

$$\begin{aligned} F(p, n, \overline{c}, \phi) &:= h_c(c, \rho) - h_c(2\overline{c}, 0) = 0, \\ G(p, n, \overline{c}, \phi) &:= h_\rho(c, \rho) - \phi - h_\rho(2\overline{c}, 0) = 0. \end{aligned} \tag{A1}$$

The Jacobian

$$J := \frac{\partial(F, G)}{\partial(\phi, \overline{c})} = - \begin{bmatrix} 0 & 2h_{cc} \\ 1 & 2h_{c\rho} \end{bmatrix}$$

satisfies $\det J = 2h_{cc} > 0$ since h is strictly convex. Therefore, by the implicit function theorem, the system (A1) defines $\overline{c}(c, \rho)$ and $\phi(c, \rho)$.

Appendix B: Admissibility of solutions implies convexity of h

We show that the admissibility conditions (19,22) imply strict convexity of the solution h.

Indeed, by (14)

$$\begin{aligned} h_{cc}(c, \rho) &= A'(\overline{c})\overline{c}_c, \\ h_{c\rho}(c, \rho) &= A'(\overline{c})\overline{c}_\rho = \left[\phi_{\overline{c}} + B'(\overline{c})\right] \overline{c}_c, \\ h_{\rho\rho}(c, \rho) &= \phi_\rho(c, \rho) + \phi_{\overline{c}}\overline{c}_\rho + B'(\overline{c})\overline{c}_\rho, \end{aligned}$$

Therefore,

$$
\begin{aligned}
|\mathrm{Hess}_{c,\rho} h| = h_{\rho\rho} h_{cc} - h_{c\rho}^2 &= A'(\overline{c})\overline{c}_c \left[\phi_\rho + \phi_{\overline{c}}\overline{c}_\rho + B'(\overline{c})\overline{c}_\rho\right] - A'(\overline{c})\overline{c}_\rho \left[\phi_{\overline{c}} + B'(\overline{c})\right]\overline{c}_c \\
&= A'(\overline{c})\overline{c}_c \left[\phi_\rho + \cancel{\overline{c}_\rho \phi_{\overline{c}} - \overline{c}_\rho \phi_{\overline{c}}} + \cancel{\overline{c}_\rho B'(\overline{c}) - \overline{c}_\rho B'(\overline{c})}\right] \\
&= A'(\overline{c})\overline{c}_c \phi_\rho > 0.
\end{aligned}
$$

The last inequality is due to the admissibility conditions $A' > 0$ and $\overline{c}_c > 0$, and due to Lemma 2 which ensures that $\phi_\rho > 0$. □

---

[1] G.-W. Wei, Q. Zheng, Z. Chen, and K. Xia, SIAM Review **54**, 699 (2012).

[2] B. Eisenberg, Biophysical journal **104**, 1849 (2013).

[3] B. Conway, "Electrochemical supercapacitors-scientific fundamentals and technological applications (chen a, wu mq, zhang xl, gao nw trans.)," (2005).

[4] P. Sharma and T. Bhatti, Energy Conversion and Management **51**, 2901 (2010).

[5] N.-S. Choi, Z. Chen, S. A. Freunberger, X. Ji, Y.-K. Sun, K. Amine, G. Yushin, L. F. Nazar, J. Cho, and P. G. Bruce, Angewandte Chemie International Edition **51**, 9994 (2012).

[6] The overall system is charge neutral, the surface charge on the wall balances the net charge in the adjacent electrolyte layer.

[7] J. Lyklema, Colloids and Surfaces A **291**, 3 (2006).

[8] Our presentation is restricted to non-ideality effects in entropy for simplicity, extension to non-ideality in enthalpy is straightforward.

[9] D. Di Caprio, Z. Borkowska, and J. Stafiej, Journal of Electroanalytical Chemistry **540**, 17 (2003).

[10] N. Gavish and K. Promislow, http://ngavish.net.technion.ac.il/files/2014/12/OnTheStructureofGenPB.pdf (2014).

[11] Y. R. Shen, J. Opt. Soc. Am. B **28**, A56 (2011).

[12] C. C. Wang, Physical Review **178**, 1457 (1969).

[13] G. Valette, J. Electroanal. Chem. **122**, 285297 (1981).

[14] M. Kilic, M. Z. Bazant, and A. Ajdari, Phys. Rev. E **75**, 021502 (2007).

[15] D. Ben-Yaakov, D. Andelman, D. Harries, and R. Podgornik, J. Phys.: Condens. Matter **21**, 424106 (2009).

[16] J. J. López-García, J. Horno, and C. Grosse, Langmuir **27**, 13970 (2011).

[17] H. O. Stern-Hamburg, S. f. Electrochemie **30**, 508 (1924).

[18] J. Bikerman, Philosophical Magazine **33**, 384 (1942).

[19] D. di Caprio, Z. Borkowska, and J. Stafiej, Journal of Electroanalytical Chemistry **572**, 51 (2004).

[20] T. Boublík, J. Chem. Phys. **53**, 471 (1970).

[21] G. Mansoori, N. Carnahan, K. Starling, and T. Leland Jr, The Journal of Chemical Physics **54**, 1523 (1971).

[22] T.-L. Horng, T.-C. Lin, C. Liu, and B. S. Eisenberg, J. Phys. Chem. B **116**, 11422 (2012).

[23] Y. Hyon, J. E. Fonseca, B. S. Eisenberg, and C. Liu, Discrete and Continuous Dynamical Systems Series B (DCDS-B) **17**, 2725 (2012).

[24] Y. Nakayama and D. Andelman, The Journal of chemical physics **142**, 044706 (2015).

[25] D. Ben-Yaakov, D. Andelman, R. Podgornik, and D. Harries, Current Opinion in Colloid & Interface Science **16**, 542 (2011).

[26] F. Booth, The Journal of Chemical Physics **19**, 391 (1951).

[27] M. M. Hatlo, R. van Roij, and L. Lue, EPL (Europhysics Letters) **97**, 28010 (2012).

[28] D. Ben-Yaakov, D. Andelman, and R. Podgornik, J. Chem. Phys. **134**, 074705 (2011).

[29] J. J. López-García, J. Horno, and C. Grosse, Langmuir **27**, 13970 (2011).

[30] M. Z. Bazant, M. S. Kilic, B. D. Storey, and A. Ajdari, Advances in Colloid and Interface Science **152**, 48 (2009).

[31] The singularity at $\alpha = 2$ is removable. The case $0 < \alpha < 1$ will be discussed in the section on charge reversal.

[32] J. Lyklema, Advances in Colloid and Interface Science **147-148**, 205 (2009).

[33] M. Quesada Pérez, E. González Tovar, A. Martín Molina, M. Lozada Cassou, and R. Hidalgo Álvarez, ChemPhysChem **4**, 234 (2003).

[34] Non-monotone charge profiles also arise in the somehow related over-screening phenomena. In this case, the charge profiles exhibits non-monotonic oscillatory *decays* as a function of the distance from the wall, which differ from phenomena observed in Figure 6 where ion charge density *increases* near the wall rather than decays. Recent works have described over-screening using symmetric models [23, 40, 41].

[35] Indeed, since $\phi(Q, \rho)$ is an even function in Q and $B' \equiv 0$, the characteristic curves are also

even functions of t, see equation (20). But $Q = A'(\overline{c})t$, and thus h is an even function of Q.

[36] As in Figure 4, the charge density profile becomes negative at high applied voltage.

[37] From a physical point of view, the validity $\epsilon(p, n) \geq \epsilon_0$ where ϵ_0 is vacuum permittivity.

[38] The admissibility of the choices of free data A and B is verified in the region in which the experimental data is available (roughly $|\rho| < 0.1$ and $c < 0.15$).

[39] K. Promislow, J. Jones, Z. Xu, N. Gavish, and A. Christlieb, ECS Transactions **50**, 161 (2013).

[40] M. Z. Bazant, B. D. Storey, and A. A. Kornyshev, Phys. Rev. Lett. **106**, 46102 (2011).

[41] A. Yochelis, J. Phys. Chem. C **118**, 5716 (2014).